PCCP

ROYAL SOCIETY OF CHEMISTRY

PAPER

Cite this: *Phys. Chem. Chem. Phys.*, 2023, **25**, 28770

Carbon dioxide adsorption to UiO-66: theoretical analysis of binding energy and NMR properties†

Michiko Atsumi, [a] Jia-Jia Zheng, [b] Erik Tellgren, [a] Shigeyoshi Sakaki *[c] and Trygve Helgaker *[a]

UiO-66 is one of the most valuable metal–organic frameworks because of its excellent adsorption capability for gas molecules and its high stability towards water. Herein we investigated adsorption of carbon dioxide (CO_2), acetone, and methanol to infinite UiO-66 using DFT calculations on an infinite system under periodic-boundary conditions and post-Hartree–Fock (SCS-MP2 and MP2.5) calculations on cluster models. Three to four molecules are adsorbed at each of four μ-OH groups bridging three Zr atoms in one unit cell (named Site I). Six molecules are adsorbed around three pillar ligands, where the molecule is loosely surrounded by three terephthalate ligands (named Site II). Also, six molecules are adsorbed around the pillar ligand in a different manner from that at Site II, where the molecule is surrounded by three terephthalate ligands (named Site III). Totally fifteen to sixteen CO_2 molecules are adsorbed into one unit cell of UiO-66. The binding energy (BE) decreases in the order Site I > Site III > Site II for all three molecules studied here and in the order acetone > methanol ≫ CO_2 in the three adsorption sites. At the site I, the protonic H atom of the μ-OH group interacts strongly with the negatively charged O atom of CO_2, acetone and methanol, which is the origin of the largest BE value at this site. Although the DFT calculations present these decreasing orders of BE values correctly, the correction by post-Hartree–Fock calculations is not negligibly small and must be added for obtaining better BE values. We explored NMR spectra of UiO-66 with adsorbed CO_2 molecules and found that the isotropic shielding constants of the ^{1}H atom significantly differ among no CO_2, one CO_2 (at Sites I, II, or III), and fifteen CO_2 adsorption cases (Sites I to III) but the isotropic ^{17}O and ^{13}C shielding constants change moderately by adsorption of fifteen CO_2 molecules. Thus, ^{1}H NMR measurement is a useful experiment for investigating CO_2 adsorption.

Received 22nd August 2023,
Accepted 29th September 2023

DOI: 10.1039/d3cp04033j

rsc.li/pccp

Introduction

The zirconium-based metal–organic framework (MOF) $[Zr_6O_4(OH)_4(bdc)_6]_n$ (bdc = benzene-1,4-dicarboxylate) was synthesized by Lillerud and coworkers and named UiO-66.[1–4] In UiO-66, one OH group bridges three Zr atoms and one bdc ligand bridges two Zr atoms, as shown in Scheme 1A, and there exist tetrahedral (Td) and octahedral (Oh) cages (Scheme 1B). The UiO-66 and related MOFs have attracted great interest as excellent functional materials, as discussed in many review articles.[5–12] One of the reasons is their exceptionally high thermal and chemical stabilities compared to other MOFs. Particularly, UiO-66 and related MOFs are stable towards water atmosphere[1,2,6,7,11,12] in contrast to other MOFs which generally exhibit poor hydrothermal stability probably due to weak metal-linker bonds. Because of their high stability towards water, UiO-66 and related MOFs are recognized as excellent materials for wastewater treatment and water harvester.[7,12]

MOFs are believed to be useful for gas adsorption, separation, and storage because of the huge surface area and controlled pore structure, as suggested previously[13] and reviewed recently.[14–18] One of the important target uses for MOFs is the capture of carbon dioxide (CO_2) molecule, as discussed in many excellent works[19–29] including reviews in the last decade.[22,24,26] However, many MOFs possessing weak metal-linker bonds are not useful for post-combustion capture of CO_2 because the

[a] *Hylleraas Centre for Quantum Molecular Sciences, Department of Chemistry, University of Oslo, Box 1033, N-0315, Oslo, Norway. E-mail: t.u.helgaker@kjemi.uio.no*

[b] *Laboratory of Theoretical and Computational Nanoscience, CAS Center for Excellence in Nanoscience, National Center for Nanoscience and Technology, Chinese Academy of Sciences, No. 11 Zhong Guan Cun Bei Yi Tiao, Beijing 100190, China*

[c] *Institute for Integrated Cell-Material Sciences, Kyoto University, Rhom Plaza R312, Kyoto-daigaku-Katsura, Nishikyo-ku, Kyoto 615-8146, Japan. E-mail: sakaki.shigeyoshi.47e@st.kyoto-u.ac.jp*

† Electronic supplementary information (ESI) available: Comparison of interaction energy of gas molecule with ligand moiety between SCS-MP2, MP2.5, and CCSD(T) (Table S1), $BE^{MP2.5}$(SCM-*i*) and $BE^{SCS\text{-}MP2}$(SCM-*i*) values (Table S2), all calculated NMR shielding constants (Table S3), all calculated skews (Table S4) (PDF). See DOI: https://doi.org/10.1039/d3cp04033j

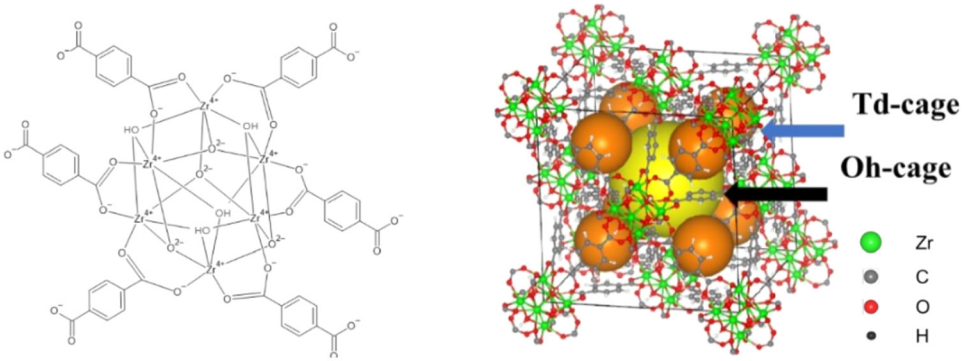

Scheme 1 Structural formula of UiO-66 $[Zr_6O_4(OH)_4(bdc)_6]_n$ (bdc = benzene-1,4-dicarboxylate) (A) and its porous structure (B).

combustion gas contains water (H_2O) in almost all cases. In this regard, UiO-66 and related MOFs are promising candidates for such post-combustion CO_2 capture because of the excellent stability towards water.[27–29] For developing further the chemistry of CO_2 adsorption to UiO-66 and related MOFs, we need detailed knowledge of CO_2 adsorption such as the adsorption position of CO_2, its binding energy with MOFs, and the strength and nature of interaction between CO_2 and MOFs. In one pioneering work, Peterson and coworkers experimentally investigated CO_2 and CD_4 adsorptions into UiO-66(Zr) and theoretically analyzed those adsorptions using the infinite UiO-66 crystal model.[30] In their work, CO_2 and CD_4 adsorption positions were determined and the relation between the host–guest interaction and the concentration of CO_2 was discussed, whereas the dispersion interaction was considered using a DFT functional including an empirical dispersion correction but no post-Hartree–Fock correction was made. Recently, Nandy and coworkers investigated NMR chemical shifts of adsorbed acetone, methanol and cyclohexane and theoretically analyzed the experimental observations using DFT calculations on a cluster model,[31] where the Zr moiety was excluded from the model to save computational cost. Because it is not easy to observe experimentally correct positions of gas molecules adsorbed to MOFs due to flexible adsorption structure, computational results of CO_2 adsorption positions, binding energies, and NMR shielding constants are of great value to the chemistry of CO_2 adsorption to UiO-66.

Here, we theoretically investigated adsorption positions and adsorption energies of CO_2, methanol and acetone molecules using DFT calculations with post-Hartree–Fock corrections and NMR chemical shifts of UiO-66 with adsorbed CO_2 molecules using DFT calculations. Our purposes here are to obtain computational knowledge of adsorption positions of CO_2 when UiO-66 is fully loaded with CO_2 molecules and binding energy of CO_2, to compare these with those of acetone and methanol, and to elucidate how much NMR shielding constants change by CO_2 adsorption. We believe that these computational results provide us with a good understanding of CO_2 adsorption to UiO-66.

Modeling and computational details

Peterson and coworkers experimentally and theoretically reported that sixty CO_2 molecules are adsorbed into one conventional unit cell of UiO-66;[30] the adsorption of sixty CO_2 molecules to one conventional unit cell corresponds to the adsorption of fifteen CO_2 molecules to one primitive unit cell. In this work, we mainly investigated the adsorption of fifteen CO_2 molecules into one primitive unit cell. In addition, we investigated the adsorption of sixteen CO_2 molecules into one primitive unit cell to make sure if the adsorption of fifteen gas molecules is the maximum; details are described below. To find the adsorption positions and orientations of CO_2 molecules, we first carried out canonical Monte-Carlo (MC) simulations using Materials Studio.[32] The standard universal force field (UFF)[33] was used to describe the van der Waals interactions between a gas molecule and UiO-66 and between gas molecules. The electrostatic interaction was evaluated using the Ewald summation method with atomic charges calculated by the charge equilibration method.[34] First, an MC simulation of 1×10^7 steps was carried out for reaching equilibration, followed by an MC calculation of 2×10^7 steps to obtain the best adsorption position(s). The positions of the CO_2 molecules can be classified into three groups, Sites I, II, and III, as discussed in the next section. In the case of acetone and methanol, the adsorption amounts have not been reported in experiment. For comparison with CO_2 adsorption, we carried out an MC simulation of UiO-66 with fifteen molecules of acetone and methanol, and found that fifteen molecules are adsorbed at Sites I, II, and III in a similar manner to the CO_2 case. Even though acetone and methanol are moderately larger than CO_2, a significant difference was not observed, as discussed below. These results suggest that the adsorption of fifteen molecules is realistic in the acetone and methanol cases.

Next, the adsorption positions and orientations of gas molecule(s) were optimized by DFT calculations under periodic boundary conditions, starting from the geometry obtained by the MC simulation. Because absorption of gas molecules to MOFs has been successfully investigated by means of DFT

calculations using functionals including dispersion correction, as reviewed elsewhere,[35,36] the Perdew–Burke–Ernzerhof (PBE) functional[37] with Grimme's D3 dispersion correction (PBE-D3)[38–40] was used here, where plane wave basis sets were employed with the cutoff energy of 500 eV and the core–valence electron interactions were described by the projector augmented-wave (PAW) method.[41,42] Γ-point sampling of the Brillouin zone was employed in all DFT calculations.

In the geometry optimization, the cell parameters and atomic positions were optimized until all atomic forces became smaller than 0.01 eV Å^{-1}. The Vienna Ab Initio Simulation Package (VASP 5.4.1)[43,44] was used for the DFT calculations under the periodic boundary conditions.

To characterize each adsorption site, we calculated the adsorption energy of one gas molecule with one unit cell, where the adsorption geometry of one gas molecule was reoptimized using DFT under the periodic boundary conditions. Although the DFT-calculated binding energies using dispersion correction functionals are in better agreement with experimental results,[35,36] the dispersion interaction is more reliably calculated with post-Hartree–Fock methods such as the Møller–Plesset second-order perturbation (MP2) method, the coupled cluster singles and doubles method with perturbative triples (CCSD(T)), or similar methods, than DFT with empirical correction for dispersion interaction. For this reason, the computational method composed of the DFT calculations on an infinite system and post-Hartree–Fock calculations on a cluster model has been used for evaluating the binding energy (BE) of gas molecule to MOF,[45–49] where the periodic boundary condition was used for DFT calculations and a cluster model is shown in Scheme 2 as an example. This method was recently named the cluster model/periodic model (CM/PM)-combined method.[49] The CM/PM-combined method resembles the ONIOM method proposed by Morokuma and coworkers.[50,51] But, the quality of computation here is slightly lower than with the two-layer ONIOM method, as described below.

In the CM/PM-combined method, the binding energy (BE) of gas molecule (G) with infinite UiO-66 is first evaluated using DFT with the PBE-D3 functional under periodic boundary conditions, as described by eqn (1):

$$\mathrm{BE}^{\text{PBE-D3:PBC}}(\mathrm{INF}) = E_{\mathrm{t}}^{\text{PBE-D3:PBC}}(\text{UiO-66·G}) - E_{\mathrm{t}}^{\text{PBE-D3:PBC}}(\text{UiO-66}) - E_{\mathrm{t}}^{\text{PBE-D3:PBC}}(\mathrm{G}) \quad (1)$$

where geometries of UiO-66 with gas molecule, UiO-66 and gas molecule are optimized and the superscript "PBE-D3:PBC" denotes that DFT calculation with the PBE-D3 functional was carried out under periodic boundary conditions (PBC) and in parentheses indicate calculated systems; for instance, INF represents an infinite system consisting of UiO-66 with an adsorbed gas molecule, and G and UiO-66·G mean, respectively, gas molecule and UiO-66 adsorbed with G molecule. The gas molecule G was calculated by DFT under periodic boundary conditions, placing one G molecule in a large box ($25 \times 25 \times 25$ Å^3). In this work, we evaluated BE for adsorption of one gas molecule and compared it among several adsorption sites; the purpose of the BE calculation is to characterize the adsorption site. For obtaining an improved BE value, we evaluated a correction ΔE_{cor} term at the post-Hartree–Fock level, as shown by eqn (2), to calculate the dispersion interaction at a higher level of theory than DFT,

$$\Delta E_{\mathrm{cor}}(\mathrm{CM}) = \mathrm{BE}^{\text{post-HF}}(\mathrm{CM}) - \mathrm{BE}^{\text{PBE-D3}}(\mathrm{CM}) \quad (2)$$

where (CM) means a cluster model and the superscripts "post-HF" and "PBE-D3" represent, respectively, that the post-Hartree–Fock method and the DFT with the PBE-D3 functional were used for evaluating the BE value. In this calculation, the structures of CM and G were taken to be the same as those in the optimized geometry of the infinite UiO-66 with adsorbed G molecule, where the dangling bonds of the cluster model were capped with hydrogen atoms; this ΔE_{cor}(CM) corresponds to the difference in the BE value between the DFT and post-Hartree–Fock calculations using a cluster model. For selecting an appropriate post-Hartree–Fock method, we compared the interaction energy of G calculated with cluster model between spin-component scaled MP2 theory (SCS-MP2)[52,53] and the MP2.5 method,[54] where the interaction energy is defined as an energy difference between the cluster model with gas molecule and the sum of the isolated cluster model and gas molecule; note their geometries were not optimized but taken to be the same as those in the total system. As shown in Table S1 of the ESI,† the MP2.5-calculated value is closer to the CCSD(T) value than the SCS-MP2 value. However, the MP2.5 calculation has a considerably larger computational cost than the SCS-MP2 calculation because the MP3 calculation is more expensive than the MP2 calculation. The cluster model employed in this work is not small, as described in the next section. Therefore, we further divided CM into several small cluster models, named SCM-*i*, as shown in Scheme 2, and calculated the $\Delta E(\mathrm{CM})_{\mathrm{cor}}$ value using the SCS-MP2 method for the CM cluster model and the MP2.5 method for the smaller cluster models SCM-*i*, as shown by eqn (3);

$$\Delta E_{\mathrm{cor}}(\mathrm{CM}) = \mathrm{BE}^{\text{SCS-MP2}}(\mathrm{CM}) - \mathrm{BE}^{\text{PBE-D3}}(\mathrm{CM}) + \sum_i \left[\mathrm{BE}^{\text{MP2.5}}(\text{SCM-}i) - \mathrm{BE}^{\text{SCS-MP2}}(\text{SCM-}i)\right] \quad (3)$$

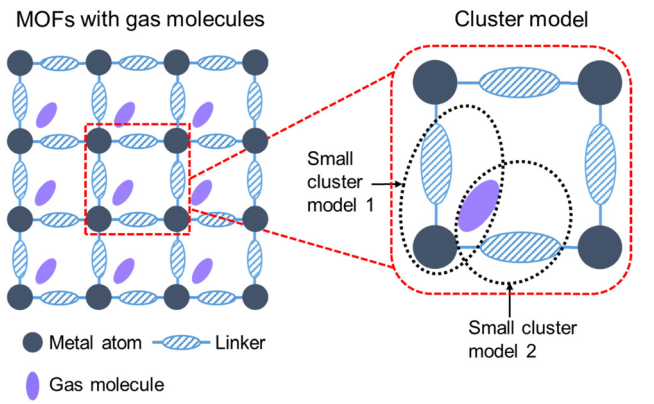

Scheme 2 Schematic representation of periodic model and cluster model.

where the geometries of SCM-*i* and G are taken to be the same as those in the optimized geometry of infinite UiO-66 with adsorbed G molecule. The second term of the right-hand side of eqn (3) indicates that the additional correction at the MP2.5 level is made using several smaller cluster models; see Scheme 2 for its example. Because of the use of smaller cluster models in addition to a cluster model, the quality of this CM/PM-combined method is a bit lower than that of the two-layer ONIOM method, as mentioned above. However, this type of correction with smaller cluster models provides reliable binding energy when the correction is made for the dispersion interaction of the van der Waals adduct.[55] The finally obtained $BE^{CM/PM}$ value is represented by eqn (4).

$$BE^{CM/PM} = BE^{PBE\text{-}D3:PBC}(INF) + \Delta E_{cor}(CM) \quad (4)$$

In the SCS-MP2 and MP2.5 calculations, the augmented correlation-consistent polarized valence double-zeta (aug-cc-pvdz) basis sets were used for all atoms except Zr, for which the Stuttgart–Dresden–Bonn basis set was used with corresponding effective core potentials.[56] The basis set superposition error (BSSE) was removed using the counterpoise method.[57] These post-Hartree–Fock calculations were carried out using Gaussian16 program.[58]

Nuclear shielding tensors were calculated using the DFT method with the PBE-D3 functional under periodic boundary conditions, where the cut-off energy of the plane wave basis sets was increased to 850 eV to improve the quality of the basis sets. For this calculation, the VASP program[43,44] was used.

Results and discussion

Adsorption positions of carbon dioxide (CO_2), acetone, and methanol

First, we carried out classical MC simulations using the primitive unit cell shown in Fig. 1, to explore whether or not fifteen CO_2 molecules can be adsorbed to UiO-66 in a reasonable manner, which moiety of UiO-66 is effective for CO_2 adsorption, and what orientation CO_2 molecules have. Starting from the obtained geometry, the geometry of UiO-66 with fifteen adsorbed CO_2 molecules was further refined by optimization with the DFT calculations under periodic boundary conditions. As shown in Fig. 1(a), fifteen CO_2 molecules can be accommodated in one unit cell in a reasonable manner. The positions and orientations of these CO_2 molecules follow the *R*3 symmetry (Fig. 1(b)). Three CO_2 molecules (blue) interact with three μ_3-OH groups bridging three Zr atoms; details are discussed below. This adsorption site is named Site I. Although each unit cell has four μ_3-HO–Zr_3 groups that construct a tetrahedra-like structure, three CO_2 molecules were adsorbed at three of those μ_3-HO–Zr_3 groups but the fourth μ_3-HO–Zr_3 group does not undergo CO_2 adsorption: the adsorption of all four sites is discussed below.

Six CO_2 molecules (brown) are found at positions different from Site I (Fig. 1(a)); this adsorption site (named Site II) is close to the terephthalate ligand. The remaining six CO_2 molecules (purple) are found at different positions (named Site III) from Sites I and II. This Site III is close to the terephthalate ligand, too. Although six CO_2 molecules are located at each of the Sites II and III in Fig. 1(b), only three of them are visible in Fig. 1(b) with remaining three CO_2 molecules being hidden behind the three visible CO_2 molecules (purple and brown) at each adsorption Site II or III.

Because the CO_2 adsorption at the fourth μ_3-HO–Zr_3 site was found not to occur by the MC simulation, we further carried out MC simulation using sixteen CO_2 molecules to investigate whether the fourth μ_3-HO–Zr_3 site undergoes CO_2 adsorption or not. The MC simulation showed that the sixteenth CO_2 molecule was not adsorbed at this site but it was found at a new site (Fig. S1 of the ESI†). The geometry optimization was further carried out using DFT under the periodic boundary conditions. In the new site, the CO_2 molecule is slightly more distant from the terephthalate ligand than at Sites II and III; it is surrounded by three CO_2 molecules at Site III.

We were concerned that the MC simulation did not show all possible CO_2 adsorptions because of insufficient simulation time. Therefore, we placed the sixteenth CO_2 molecule at the Site I near the fourth μ_3-HO–Zr_3 site and performed the geometry optimization with DFT under the periodic boundary conditions. This CO_2 molecule is bound well at the μ_3-HO–Zr_3 site; see Fig. S1(A) (ESI†). The binding energy $BE^{PBE\text{-}D3:PBC}(INF)$ at Site I (-11.51 kcal mol^{-1}) is larger in magnitude than that (-9.38 kcal mol^{-1}) at the new site.[59] These results strongly suggest that four CO_2 molecules are adsorbed at four Site Is in

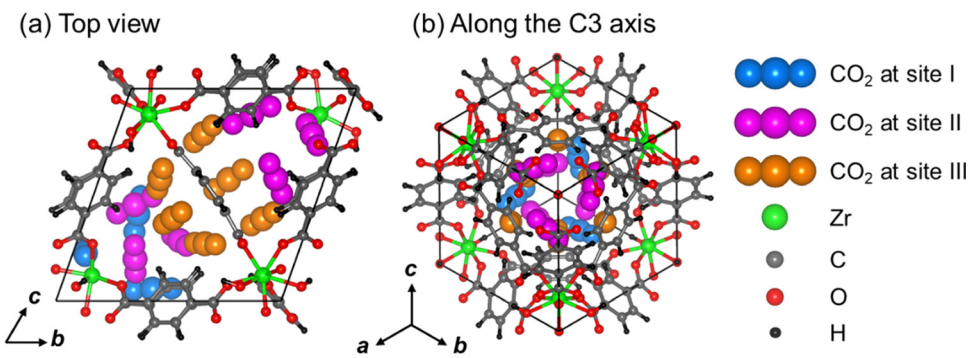

Fig. 1 (a) Top view of the optimized structure for CO_2 adsorption into UiO-66, where 15 CO_2 molecules were adsorbed at three different sites, and (b) side-view along the C_3 axis.

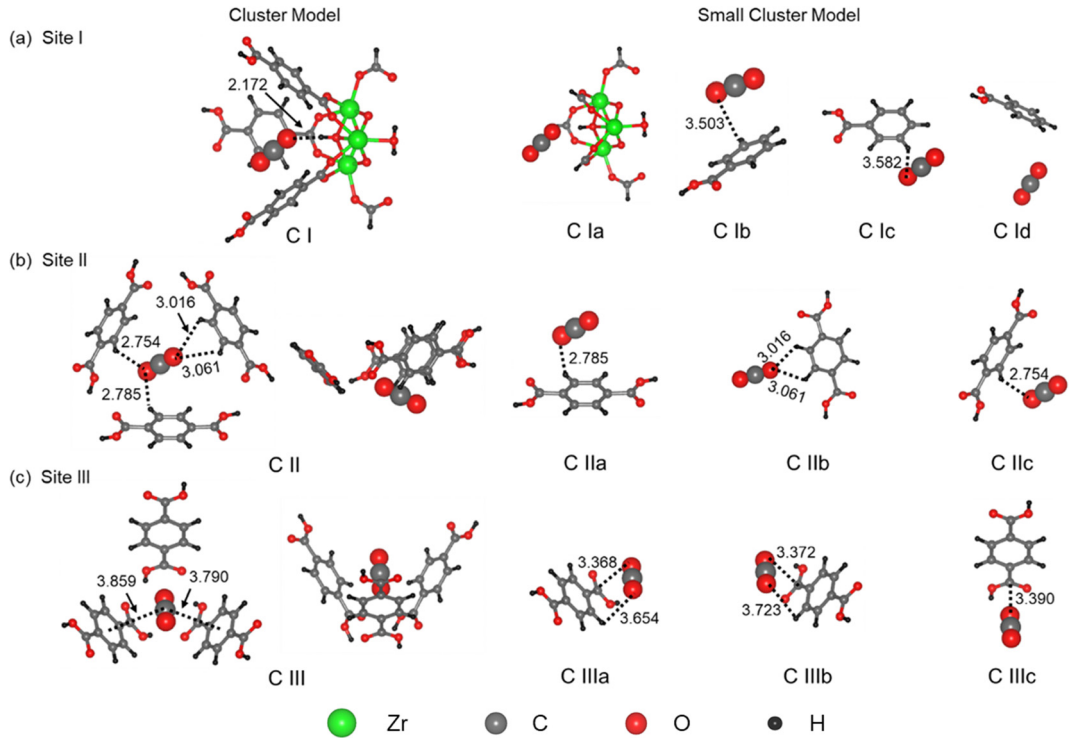

Fig. 2 Cluster models and small cluster models of CO_2 adsorption at Sites I, II, and III, where the terephthalate linkers are modeled by terephthalic acids. The numbers in the figure represent distances in angstrom.

one primitive unit cell and totally sixteen CO_2 molecules are adsorbed into one primitive unit cell. It is an important issue how many CO_2 molecules can be adsorbed into UiO-66 and a further careful study is needed. However, we focus here on the adsorption of fifteen CO_2 molecules according to the previous study,[30] because the sixteenth CO_2 adsorption influences little the other CO_2 adsorption at Site I, as shown in Fig. S1 (ESI†), and the adsorption structure obtained for one CO_2 molecule at each adsorption site was employed for characterization of each adsorption site after re-optimization of the adsorption structure.

At Site I, three CO_2 molecules are bound with three μ_3-HO–Zr_3 groups; one of them is shown by the cluster model **C I** and the small cluster model **C Ia** in Fig. 2(a). This adsorption site corresponds to the Tc_{OH} site in the previous report.[30] The optimized distance (2.172 Å) between the O atom of CO_2 and the H atom of the μ_3-OH is shorter than the experimental value (2.40 Å)[30] but agrees with the previously optimized value (2.19 Å) by DFT calculation when fifteen CO_2 molecules are adsorbed to one unit cell.[30,60] This distance is much shorter than the O–H distance (3.503 Å to 3.582 Å) between the oxygen atom of CO_2 and the hydrogen atom of the terephthalate ligand (**C Ib** and **C Ic** in Fig. 2(a)), the reason for which is discussed below. The CO_2 molecule is parallel to one C_6H_4 ring of terephthalate ligand (**C Ib** in Fig. 2(a)) to form an attractive π–π interaction with the C_6H_4 ring. However, the interactions with the other C_6H_4 rings seem weak because of the long distance and unfavorable orientation (**C Ic** and **C Id** in Fig. 2(a)). These features suggest that the interaction between the CO_2 and the terephthalate ligands is weak in Site I.

At Site II, the top view at the left-end shows that the adsorbed CO_2 molecule is surrounded by three C_6H_4 rings of terephthalate ligands but only loosely so, as shown by **C II** of Fig. 2(b). This adsorption site corresponds to the Ow site (window between two octahedral cages) previously defined.[30] The negatively charged oxygen atom of the CO_2 approaches two positively charged hydrogen atoms of the two C_6H_4 rings; the distances are 2.785–2.754 Å (**C IIa** and **C IIc**). This electrostatic interaction is not strong because the atomic charge of the hydrogen atom is moderate. The oxygen atom of the CO_2 is very distant from the hydrogen atoms of the remaining C_6H_4 ring (**C IIb**) and the CO_2 molecule is not parallel with the C_6H_4 rings, suggesting that the π–π interaction is weak. Overall, the interaction between CO_2 and the three terephthalate ligands is weak at Site II.

At Site III, each CO_2 molecule is surrounded by three C_6H_4 planes of terephthalate ligands; see **C III** in Fig. 2(c). The top view and side view of **C III** show that the CO_2 molecule is parallel to two C_6H_4 planes, with rather long distances between the carbon atom of the CO_2 and the center of these two C_6H_4 planes of 3.790 Å and 3.859 Å. However, the CO_2 is almost perpendicular to the remaining C_6H_4 ring. This adsorption site corresponds to Wt site (window between tetrahedral and octahedral cages) previously found;[30] Fig. S2 in the ESI† shows more clearly this structure from a different direction. The smaller cluster models **C IIIa** and **C IIIb** show that one negatively charged oxygen atom of CO_2 resides above the positively charged carboxyl carbon atom and the other oxygen atom resides above the positively charged hydrogen atom.

Despite the long C–O distance (3.388 Å and 3.372 Å in **C IIIa** and **C IIIb**, respectively) and the long O–H distance (3.654 Å and 3.723 Å in **C IIIa** and **C IIIb**, respectively), these structural features induce an attractive electrostatic interaction between the CO_2 and the terephthalate ligands, recalling that CO_2 is non-polar but has a quadrupole moment. The cluster model **C IIIc** indicates that the oxygen atom of the CO_2 approaches the carboxyl carbon atom in an almost perpendicular manner to the remaining C_6H_4 ring, contributing to the electrostatic interaction because the carboxyl carbon atom is positively charged and the quadrupole moment of CO_2 contributes to the electrostatic interaction with the positively charged carbon atom. These geometrical features suggest that the CO_2 adsorption occurs more strongly at Site III than at Site II, as discussed below.

We optimized the adsorption structures of acetone and methanol in a similar way. Similar to the CO_2 case, three adsorption sites are found for both acetone and methanol; see Fig. 3. At Site I, the O–H distance between the oxygen atom of acetone/methanol and the hydrogen atom of the μ_3-OH group (1.811 Å and 1.818 Å, respectively) is considerably shorter than for CO_2 (2.172 Å). These shorter distances result from the stronger Lewis basicity of the oxygen atom in acetone and methanol than in CO_2; since the μ_3-OH moiety is a Brønsted acid, the interaction between the oxygen atom of these three gas molecules and the μ_3-OH group depends on the basicity of the gas molecule. The oxygen atomic charge gets more negative in the order CO_2 ($-0.21e$) ≪ methanol ($-0.64e$) < acetone ($-0.77e$), suggesting that the Lewis basicity increases in this order. An additional factor is the polarity of the gas molecule; acetone and methanol are polar but CO_2 is non-polar. Having a stronger Lewis basicity and a larger polarity than CO_2, acetone and methanol can form a stronger electrostatic attraction with the polar Zr–μ-OH moiety than does CO_2 and approach more closely the HO–Zr moiety to induce the larger binding energies than does CO_2, as discussed in the next section.

At Site II, the oxygen atom of acetone interacts with two terephthalate ligands through the positively charged hydrogen atom, and one C–H bond of one methyl group approaches the C_6H_4 ring to form a CH–π interaction, as shown by the middle structure in Fig. 3(a). On the other hand, methanol does not form a similar electrostatic interaction between the hydrogen atom of terephthalate ligand and the oxygen atom of methanol, as shown by the middle structure in Fig. 3(b). Instead, methanol forms one OH–π interaction between its OH group and one C_6H_4 ring and two CH–π interactions between the CH bonds of the methyl group and the C_6H_4 rings; however, these CH–π interactions are weak because of a longer distance and unfavorable orientation. In addition, one C–H bond forms electrostatic interactions with two oxygen atoms of carboxyl groups of terephthalate ligands (Fig. S4, ESI†).

At Site III, two methyl groups of acetone form two CH–π interactions with the C_6H_4 rings of the ligands, one strongly and one weakly (Fig. 3a; bottom). Its oxygen atom interacts with

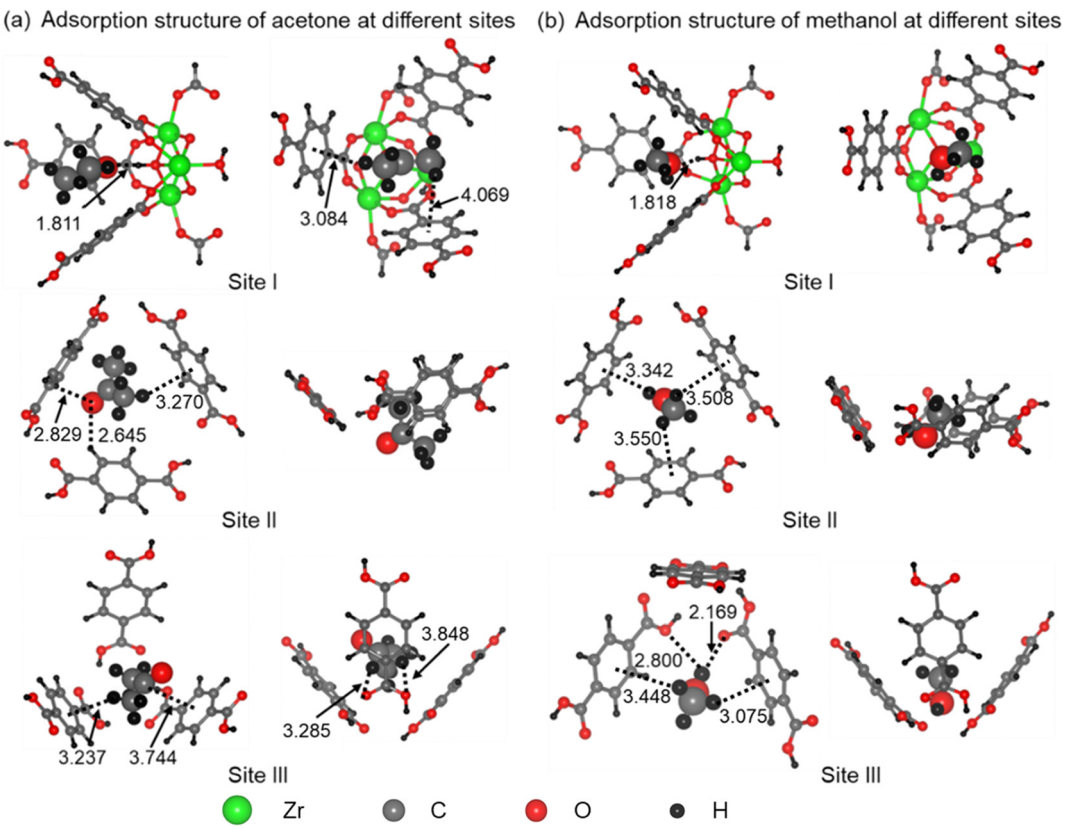

Fig. 3 Adsorption structures of acetone (a) and methanol (b) into UiO-66 at sites I, II, and III. Distances are presented in angstrom.

two CH bonds of two C_6H_4 rings, one strongly and one weakly (Fig. S3 in ESI†). In the case of methanol, the oxygen atom does not form any electrostatic interaction with the hydrogen atom of the terephthalate ligand but the protonic hydrogen atom of the methanol OH group forms one strong and one weak hydrogen-bonding-like interactions with two oxygen atoms of the carboxyl groups of the ligands (Fig. 3b, bottom). The methyl group also approaches the C_6H_4 rings to form one strong CH–π and one weak CH–π interactions. All these intermolecular interactions seem reasonable.[61]

Adsorption energies of CO_2, acetone and methanol molecules

In the chemistry of gas adsorption to MOF, the adsorption energy is an important property but its correct evaluation is difficult for several reasons: (i) the dispersion interaction is important particularly when MOF has no open metal site; (ii) the electrostatic interaction is important for polar molecules because the infinitely periodic structure of MOF may strengthen or weaken it at a given position. In the case of UiO-66, both factors must be taken into consideration because UiO-66 does not have an open metal site and also has highly polarized Zr–O coordination bonds. Although CO_2 is a non-polar molecule, its adsorption energy would depend on electrostatic potential of MOF because CO_2 has negatively charged oxygen atoms, a positively charged carbon atom, and quadrupole moment. Hence, both the periodic structure of UiO-66 and the dispersion interaction must be evaluated correctly. It is likely that the electrostatic interaction can be reliably described by DFT. For the dispersion interaction, however, post-Hartree–Fock methods such as the MP2, SCS-MP2, and CCSD(T) are more reliable than DFT. Here, we employed the CM/PM-combined method consisting of DFT calculations of the infinite structure of UiO-66 under the periodic boundary conditions and SCS-MP2 and MP2.5 calculations of cluster models, as described in the section of Modeling and Computational Details. To characterize three adsorption sites, we evaluated the adsorption energy of one gas molecule here.

CO_2 at site I

At Site I, CO_2 molecule approaches the bridging μ_3-OH ligand coordinating with three Zr atoms. Since the Zr–O coordination bond considerably influences the protonic character of the hydrogen atom, we included the Zr moiety in the cluster model **C I**; see Fig. 2(a). As discussed in the section of Modeling and Computational Details, we wanted to calculate the BE value using the MP2.5 method since it reproduces the CCSD(T)-calculated interaction energy between CO_2 and the ligand moiety better than does the SCS-MP2 method. However, because of the presence of MP3 component, the MP2.5 calculation is too expensive for the cluster model **C I**. We therefore divided the cluster model **C I** into several smaller models, **C Ia**, **C Ib**, **C Ic**, and **C Id** (Fig. 2(a)). We likewise divided the cluster models **C II** and **C III** into smaller cluster models (Fig. 2(b) and (c)). The $BE^{PBE\text{-}D3}$ (INF) value obtained by eqn (1) is −7.68 kcal mol^{-1} (a negative value means stabilization energy), which is the largest among the three adsorption sites, as shown in Table 1. The PBE-D3-calculated $BE^{PBE\text{-}D3}$(CM) value of the cluster model **C I** is more negative than the corresponding SCS-MP2-calculated $BE^{SCS\text{-}MP2}$(CM) value by 1.19 kcal mol^{-1}, suggesting that the PBE-D3 method overestimates the adsorption energy and a post-Hartree–Fock correction is needed for evaluating correctly the BE value.

We then evaluated the correction term $\Delta BE_{cor}^{MP2.5-SCS\text{-}MP2}$(SCM) using small cluster models **C Ia**, **C Ib**, **C Ic**, and **C Id**. This term is about 1 kcal mol^{-1}, indicating that the SCS-MP2 method tends to underestimate BE values and that the MP2.5 correction must be added to recover the underestimated $BE^{SCS\text{-}MP2}$ (SCM) value to some extent. A similar result, the underestimation of BE by the

Table 1 DFT-calculated binding energy ($BE^{PBE\text{-}D3:PBC}$(INF)) of infinite system, SCS-MP2- and PBE-D3-calculated binding energies ($BE^{SCS\text{-}MP2}$(CM) and $BE^{PBE\text{-}D3}$(CM)) using cluster model (**C I**, **C II**, or **C III**), correction term of BE value by MP2.5 calculations using small cluster models $\Delta BE_{cor}^{MP2.5-SCS\text{-}MP2}$(SCM), and $BE^{CM/PM}$ calculated by the CM/PM-combined method (in kcal mol^{-1})

	Infinite system	Cluster model (CM)		Small cluster model (SCM)	CM/PM-combined method
	$BE^{PBE\text{-}D3:PBC}$(INF)	$BE^{PBE\text{-}D3}$(CM)	$BE^{SCS\text{-}MP2}$(CM)	$\Delta BE_{cor}^{MP2.5-SCS\text{-}MP2}$ (SCM)	$BE^{CM/PM}$
CO_2					
Site I	−7.68	−7.04 (with **C Ia**)	−5.85 (with **C Ia**)	−0.92 (with **C Ia**)	−7.41 (with **C Ia**)
		−5.08 (without **C Ia**)	−3.88 (without **C Ia**)	−0.52 (without **C Ia**)	−7.00 (without **C Ia**)
Site II	−4.19	−3.55	−1.87	−0.48	−2.99
Site III	−6.19	−5.41	−4.25	−0.47	−5.50
Acetone					
Site I	−18.70	−9.77	−7.60	−1.45	−17.99
Site II	−10.99	−9.17	−5.81	−1.41	−9.03
Site III	−12.50	−8.44	−5.97	−1.09	−11.11
Methanol					
Site I	−14.71	−6.53	−4.24	−1.25	−13.67
Site II	−8.80	−7.03	−4.50	−0.91	−7.18
Site III	−9.52	−8.17	−4.93	−1.34	−7.62

[a] $\Delta BE_{cor}^{MP2.5-SCS\text{-}MP2}(SCM) = \sum_i \left[BE^{MP2.5}(SCM\text{-}i) - BE^{SCS\text{-}MP2}(SCM\text{-}i)\right]$; $BE^{MP2.5}$(SCM-*i*) and $BE^{SCS\text{-}MP2}$(SCM-*i*) values are presented in Table S2 of the ESI.

MP2 method and its partial recovery by the CCSD(T) method, was reported in a theoretical work of CO_2 adsorption to MOF.[47] In addition, we calculated the post-Hartree–Fock correction without the small cluster model **C Ia** which contains the μ_3-HO–Zr moiety (Fig. 2(a)). The $BE^{PBE\text{-}D3}$(CM) value without **C Ia** is considerably smaller than the $BE^{PBE\text{-}D3}$(CM) value with **C Ia** by 1.19 kcal mol^{-1}, showing that the Zr moiety must be contained in the cluster model to obtain a reliable BE energy. However, the $BE^{SCS\text{-}MP2}$(CM) value of the cluster model without **C Ia** is also considerably smaller than the $BE^{PBE\text{-}D3}$(CM) value with **C Ia** by 2.0 kcal mol^{-1}. The $\Delta BE^{MP2.5\text{-}SCS\text{-}MP2}$(SCM) value obtained for the small cluster models **C Ib**, **C Ic**, and **C Id** without **C Ia** is also smaller by 0.4 kcal mol^{-1} than that obtained for all the small cluster models, **C Ia**, **C Ib**, **C Ic**, and **C Id**. The total correction ((−1.19 − (−2.0) −0.40) kcal mol^{-1}) is −0.41 kcal mol^{-1}. As a result, the $BE^{CM/PM}$ value is −7.41 kcal mol^{-1} when **C Ia** is included and 7.00 kcal mol^{-1} when **C Ia** is excluded, indicating that the post-Hartree–Fock correction is about 3.5% of $BE^{PBE\text{-}D3:PBC}$(INF) when **C Ia** is involved and 8.9% of $BE^{PBE\text{-}D3:PBC}$(INF) when **C Ia** is not. These results imply that the interaction with the μ_3-HO–Zr_3 moiety is important for obtaining the BE value of CO_2 with UiO-66 but that the post-Hartree–Fock correction is not very large for this **C Ia** (about 5% of $BE^{PBE\text{-}D3:PBC}$(INF)). This is reasonable because the electrostatic interaction between the negatively charged oxygen atom of CO_2 and the positively charged hydrogen atom of the μ_3-HO–Zr_3 moiety contributes largely to the BE(CM) and it can be evaluated well at the DFT level. Therefore, the post-Hartree–Fock correction of **C Ia** is not very important at Site I compared to other Sites II and III.

CO_2 at site II

At Site II, one oxygen atom of CO_2 interacts with two C–H bonds of two C_6H_4 rings of the terephthalate ligands and the remaining oxygen atom interacts with two C–H bonds of one C_6H_4 ring (**C IIa** and **C IIc** in Fig. 2). Although the electrostatic interaction plays an important role in such a case, it is likely that the dispersion interaction is also important because the π-electron system of CO_2 approaches the π-electron system of the C_6H_4 moieties (see **C IIa** and **C IIc** in Fig. 2(b)). This is the reason why we employed the post-Hartree–Fock calculations using cluster models in this work. We found two important results, as follows.

The first one is the somewhat large difference between $BE^{PBE\text{-}D3:PBC}$(INF) and $BE^{PBE\text{-}D3:PBC}$(CM), where CM is a cluster model of Site II shown in Fig. 2(b); the $BE^{PBE\text{-}D3:PBC}$(CM) is about 15% smaller than the $BE^{PBE\text{-}D3:PBC}$(INF). This result shows that the use of a cluster model is not good for obtaining a reliable BE value. The other is the considerably large difference between the $BE^{PBE\text{-}D3}$(CM) and $BE^{SCF\text{-}MP2}$ (CM) values (Table 1), suggesting that the dispersion interaction must be evaluated at the post-Hartree–Fock level. As a result, the BE value decreases by 1.68 kcal mol^{-1} (−1.87 kcal mol^{-1} − (−3.53 kcal mol^{-1})) by the SCS-MP2 correction. The $\Delta BE^{MP2.5\text{-}SCS\text{-}MP2}$(SCM) term partially recovers this value by 0.48 kcal mol^{-1}. The final $BE^{CM/PM}$ value with all corrections is considerably smaller than the $BE^{PBE\text{-}D3:PBC}$(INF) value by 1.20 kcal mol^{-1} (Table 1). The post-Hartree–Fock correction is considerably large, about 28.6% of the $BE^{PBE\text{-}D3:PBC}$(INF) value.

CO_2 at site III

At Site III, the $BE^{PBE\text{-}D3:PBC}$(INF) value is larger than that of Site II but smaller than that of Site I (Table 1). The $BE^{PBE\text{-}D3}$(CM) value for the cluster model **C III** is larger than the $BE^{SCS\text{-}MP2}$(CM) value as in Site II, whereas the difference between these two values is considerably smaller than in Site II; for instance, the $BE^{SCS\text{-}MP2}$(CM) value is about 50% of the $BE^{PBE\text{-}D3}$(CM) value for Site II but about 80% for Site III. The $\Delta BE^{MP2.5\text{-}SCS\text{-}MP2}$(SCM) value (−0.47 kcal mol^{-1}), the sum of correction terms for the small cluster models **C IIIa**, **C IIIb** and **C IIIc**, is similar to that of Site II. As a result, the BE value is recovered by 0.47 kcal mol^{-1} and the final $BE^{CM/PM}$ value (−5.50 kcal mol^{-1}) is somewhat smaller than the $BE^{PBE\text{-}D3:PBC}$(INF) value by 0.69 kcal mol^{-1}. The post-Hartree–Fock correction is about 11.1% of the $BE^{PBE\text{-}D3:PBC}$(INF) value. Although the post-Hartree–Fock correction is significant, it is much smaller than at Site II. This is reasonable because the electrostatic attraction is larger in the two small cluster models (**C IIIa** and **C IIIb**) at Site III than at Site II in which an electrostatic attraction is found only in **C IIb**: In other words, the electrostatic interaction contributes more to the adsorption energy at Site III than at the Site II.

Here, we make comparison between the experimentally reported isosteric heat of the first CO_2 adsorption and the calculated binding energy of the first CO_2 adsorption at Site I because it is likely that the first CO_2 molecule is adsorbed at Site I due to the largest binding energy; note that the comparison with other experimental values is difficult because of the lack of information about the number of adsorbed CO_2 molecules at Sites I, II, and III. The calculated $BE^{CP/PM}$ value for the first CO_2 adsorption is 7.41 kcal mol^{-1} (= 31.0 kJ mol^{-1}) with the SCS-MP2 and MP2.5 corrections of **C Ia** and 7.01 kcal mol^{-1} (= 29.3 kJ mol^{-1}) without the corrections of **C Ia**. These calculated values are moderately larger than the experimental values,[62–64] similar to the previously calculated value (29.9 kJ mol^{-1}) by Zhou *et al.*,[65] but moderately smaller than the calculated value (33.3 kJ mol^{-1}) by Peterson *et al.*[30] Though the difference between the calculated value and the experimental one is not bad considering the large size, flexible adsorption position, and contribution of many weak interactions, further theoretical efforts are needed for better estimation of the binding energy.

Acetone and methanol at sites I, II, and III

We evaluated the adsorption energies of acetone and methanol in a similar way to that of CO_2, whose cluster models and smaller cluster models are shown in Fig. S3 and S4 of the ESI.† In these gas molecules, we did not include the μ_3-HO–Zr_3 moiety in the cluster models because the post-Hartree–Fock correction is not very important for the interaction with the μ_3-HO–Zr_3 moiety in the CO_2 case; this is reasonable because the electrostatic interaction largely contributes to the BE value at Site I and the DFT method is likely to describe well the

electrostatic interaction. In both acetone and methanol, the largest $BE^{CM/PM}$ value is obtained at Site I as for CO_2; see Table 1. These results clearly show that Site I is the most important adsorption site in UiO-66 and that the μ_3-OH group plays an important role in gas adsorption. Consistent with the large $BE^{PBE\text{-}D3:PBC}$(INF) and $BE^{CP/PM}$ values for Site I, the O–H distance is rather short (1.811 Å and 1.818 Å, respectively, as discussed above and shown in Fig. 3). The $BE^{CM/PM}$ value decreases in the order Site I > Site III > Site II, as for the CO_2 case.

Summary of BE values of all gas molecules at all sites

First, we compare here the binding energy between the post-Hartree–Fock corrected $BE^{CM/PM}$ and the DFT-calculated $BE^{PBE\text{-}D3:PBC}$ values, as shown in Fig. 4. Apparently, all $BE^{CM/PM}$ values are less negative than the $BE^{PBE\text{-}D3:PBC}$ values, indicating that the post-Hartree–Fock corrections decrease the binding energy; see also Table 1. However, it is noted that all $BE^{CM/PM}$ values are, to a good approximation, directly proportional to the $BE^{PBE\text{-}D3:PBC}$ values, indicating that the DFT-calculated binding energy under periodic boundary conditions is useful for semi-quantitative discussion of the binding energy.

Next, we compare the binding energy at Sites I, II, and III, and for CO_2, acetone, and methanol. The $BE^{CM/PM}$ values at Sites I, II, and III decrease in the order acetone > methanol > CO_2. At Site I, this decreasing order of the binding energy is consistent with the calculated O–H distances discussed above and with our expectation based on the polarity and the negative charge of the oxygen atom of the gas molecule, as discussed above. For all three molecules, the $BE^{CM/PM}$ value decreases in the order Site I > Site III > Site II. This decreasing order can be understood in the following manner: At Site I, the negatively charged oxygen atom of the gas molecule forms a Brønsted-acid–Lewis-base interaction with the protonic hydrogen atom of the μ-OH group. It is likely that this is stronger than the CH–π, OH–π, and CH–O interactions as it represents the acid–base interaction between the protonic hydrogen atom of the μ-OH group and the negatively charged oxygen atom of gas molecule: Indeed, the decreasing order of the $BE^{CP/MP}$ value at Site I is parallel to the decreasing order of the negative charge of the oxygen atom of gas molecule (discussed above). In addition, CO_2 forms one π–π interaction with one C_6H_4 ring, and both acetone and methanol form CH–π interaction between one CH bond of their methyl groups and the C_6H_4 ring (Fig. 3a and b). These interactions contribute to the binding energy but they are weaker than the acid–base interaction.

At Sites II and III, these three gas molecules form typical intermolecular interactions such as CH–π, OH–π, CH–O and OH–O interactions. Although the comparison of those weak intermolecular interactions is difficult, Site III seems better than Site II because the number of intermolecular interactions is larger in Site III than in Site II; in other words, these gas molecules have better orientation and position in Site III for intermolecular interactions than in Site II.

Here, we have two important conclusions; (i) the post-Hartree–Fock correction always decreases the binding energy calculated by DFT under periodic boundary conditions. However, the DFT-calculated binding energy $BE^{PBE\text{-}D3:PBC}$ is useful for semi-quantitative discussion. And, (ii) UiO-66 is useful for adsorption of gas molecules with Lewis base character because of the presence of the μ-OH group, as reported experimentally.[65] If its protonic H atom is removed, the anionic μ-O group appears, which is useful for interacting with the Lewis acid and metal cation. Indeed, one experimental work recently succeeded in incorporating Cu(II) ions on the O group in UiO-66 and enhancing the adsorption of NH_3 molecules.[66]

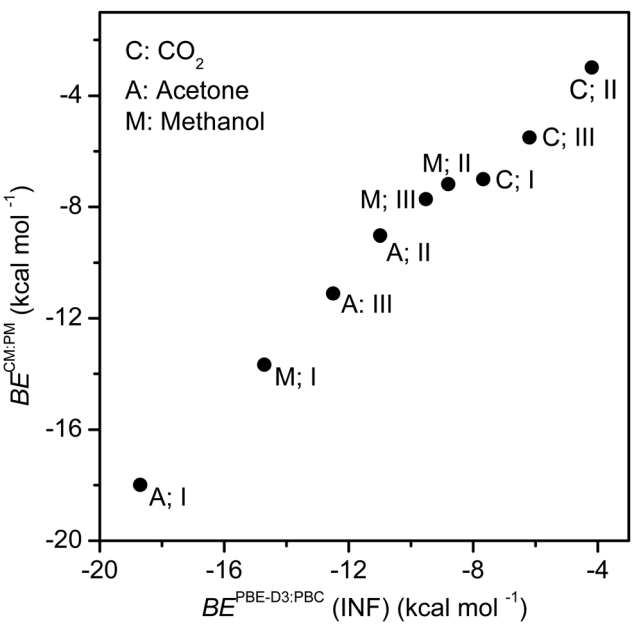

Fig. 4 Comparison between $BE^{CM/PM}$ and $BE^{PBE\text{-}D3:PBC}$(INF) values for CO_2, acetone, and methanol.

NMR shielding tensors

Here, we focus on the changes in NMR shielding constants by CO_2 adsorption, bearing in mind that the CO_2 adsorption to MOFs is a promising CO_2 capture technique and that NMR measurement is expected to be useful for investigating CO_2 adsorption.[31,67,68] In Fig. 5, the isotropic shielding constants $\sigma_{iso} = (\sigma_{11} + \sigma_{22} + \sigma_{33})/3$ are plotted for different numbers of adsorbed CO_2 molecules; details of the NMR shielding tensors are presented in Table S3 of the ESI.† We show violin plots as a visual support in Fig. 5, because distributions are not unimodal and therefore poorly summarized by simple statistics such as mean values and standard deviations. In this work, we evaluated NMR shielding constants but not the corresponding NMR chemical shifts relative to the reference materials for following reasons: (1) the calculation of liquid water, which is the reference of ^{17}O chemical shift, is not easy and the value is always qualitative, and (2) the changes in NMR chemical shifts by CO_2 adsorption can be discussed well using relative values to the NMR shielding constants of UiO-66 without CO_2 adsorption. Here, we mainly discuss whether the NMR shielding

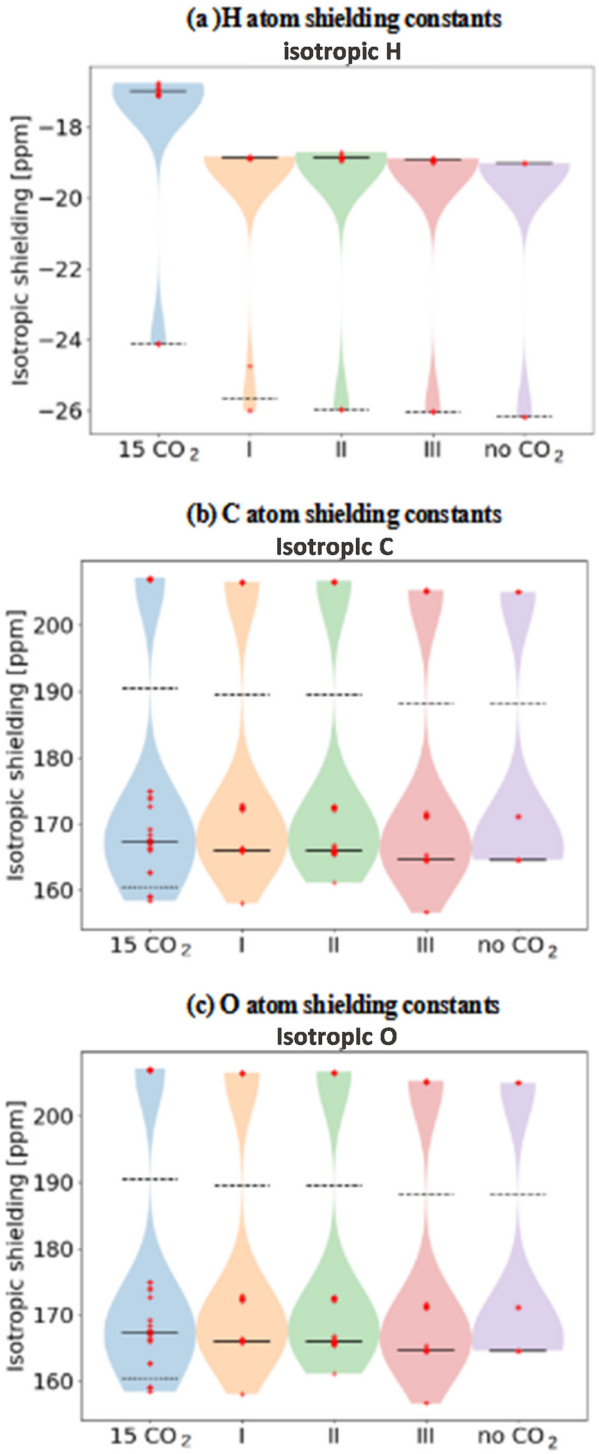

Fig. 5 The calculated nuclear shielding constants of hydrogen atom[a] (a), carbon atom[b] (b), and oxygen atom[c] (c) in UiO-66 with adsorbed CO_2. From left to right in each subplot, the shielding constants with 15 adsorbed CO_2, 1 CO_2 at Site I, 1 CO_2 at Site II, 1 CO_2 at Site III, and no CO_2, respectively, are shown. Data points are shown as crosses. [a]Solid line and dashed line represent respectively mean values of hydrogen atoms bound to a carbon atom and all other hydrogen atoms. [b]Solid line, dashed line, and dotted line represent respectively mean values of carbon atoms bound to a hydrogen atom and all carbon atoms except that of CO_2. [c]Solid line and dotted line represent respectively mean values of all oxygen atoms except CO_2 and oxygen atoms of adsorbed CO_2 molecule.

constants change upon the CO_2 adsorption into UiO-66 or not and how much they change.

Proton shielding constants

The hydrogen atoms of UiO-66 without CO_2 adsorption exhibit bimodal NMR shielding constants with twenty symmetrically equivalent hydrogen atoms around −19 to −20 ppm and four symmetrically equivalent hydrogen atoms at −26 ppm; see the violin plot at "no CO_2" column on the right-end of Fig. 5(a). These values slightly shift upward by adsorption of one CO_2 molecule at Sites I, II, and III; see "I", "II", and "III" columns presented on middle in Fig. 5(a). Upon CO_2 adsorption, the symmetrical equivalence disappears and the signal at −19 ppm becomes a cluster composed of several lines nearby to each other. However, the violin plot and the mean values do not significantly change, where the mean value of hydrogen atoms bound to the carbon atoms and that of the other hydrogen atoms are presented respectively by a solid and dashed lines in Fig. 5(a). When fifteen CO_2 molecules are adsorbed, the NMR shielding constants of the hydrogen atoms substantially shift upward; see the violin plot at "15 CO_2" column on the left-end in Fig. 5(a). In addition, the cluster of shielding constants at the upper (less negative) end broadens more than it does upon adsorption of one CO_2 molecule, suggesting that the geometry deformation occurs more by adsorption of fifteen CO_2 molecules than that by one CO_2 molecule. As a result, the violin plot and the mean value of oxygen atoms of CO_2 change somewhat.

All these computational results strongly suggest that proton NMR measurements can provide us with valuable information in studying CO_2 adsorption to UiO-66 when the CO_2 adsorption fully occurs.

Carbon shielding constants

Without CO_2 adsorption, the carbon atoms of UiO-66 exhibit non-unimodal shielding constants at three sites in the same way as for the hydrogen atoms, 165 ppm (twenty-four atoms), 171 ppm (twelve atoms), and 205 ppm (twelve atoms), as shown at "no CO_2" column on the right-end of Fig. 5(b). The ^{13}C NMR chemical shifts were experimentally observed at 129 ppm, 137 ppm, and 171 ppm and previously calculated at 130.8 ppm, 137.1 ppm, and 171.0 ppm by DFT using the PBE functional.[67] These were assigned to the aromatic carbon atom bound to the hydrogen atom, the aromatic *ipso* carbon atoms bound to the carboxyl (–COO) group, and the carbonyl carbon atoms, respectively. The ^{13}C NMR shielding constants calculated here agree with the assignments of the former work[67] and the differences between these three NMR shielding constants are almost the same as those of the experimentally observed chemical shifts.[67] When one CO_2 molecule is adsorbed, the ^{13}C NMR shielding constants of the adsorbed CO_2 molecule is calculated in the range 156–163 ppm; see the violin plot at the "I", "II", and "III" columns in Fig. 5(b). The shielding constant below 165 ppm depends moderately on the CO_2 adsorption at Sites I, II, and III. When fifteen CO_2 molecules are adsorbed to UiO-66, the ^{13}C NMR shielding constants at 165 ppm (due to carbons bound to hydrogens) broaden to a cluster of values in

the interval of 165–170 ppm, respectively, as shown by the "15 CO_2" column at the left-end of Fig. 5(b). Similarly, the peak initially at 171 ppm shifts broadens to an interval 173–175 ppm upon absorption. Although the violin plot and the mean values do not change very much upon adsorption of fifteen CO_2 molecules, the broadening of ^{13}C NMR shielding constants around 165–170 ppm and 173–175 ppm can be used as a signal for full CO_2 adsorption.

Oxygen shielding constants

The oxygen atoms in UiO-66 without CO_2 adsorption exhibit shielding constants around 66 ppm (one atom), 325 ppm (twenty-four atoms), and 459 ppm (two atoms), as shown at the right-end (the "no CO_2" column) of Fig. 5(c). The peak at 66 ppm was not experimentally observed, but this is not unreasonable because only one oxygen atom contributes to it and the experimental signal should be very small. Adsorption of one CO_2 molecule at Sites I, II, and III slightly changes the peaks around 325 and 459 ppm and broadens the peak around 66 ppm to the interval 66–105 ppm; see the "I", "II", and "III" columns in Fig. 5(c). When fifteen CO_2 molecules are adsorbed, the cluster around 100 pm broadens, as shown by the "15 CO_2" column at the left-end of Fig. 5(c). In addition, the violin plot around 100 ppm changes considerably when fifteen CO_2 molecules are adsorbed. These results indicate that the ^{17}O NMR spectroscopy is effective for studying CO_2 adsorption into UiO-66 for full CO_2 adsorption case. Indeed, the ^{17}O NMR measurement has been employed for investigating MOFs.[68]

Shielding anisotropy

Adsorption of CO_2 also manifests itself in the anisotropy of the nuclear shielding tensor. With the conventional relation $\sigma_{11} > \sigma_{22} > \sigma_{33}$ for the eigenvalues of the nuclear shielding tensors, we define the skew by,[69]

$$\kappa = 3\frac{\sigma_{iso} - \sigma_{22}}{\sigma_{11} - \sigma_{33}} = \frac{\sigma_{11} + \sigma_{33} - 2\sigma_{22}}{\sigma_{11} - \sigma_{33}} \quad (5)$$

where either shielding constants or chemical shifts can be used. Although the isotropic value is important for the location of the NMR spectrum, the skew κ is important for the line shape. Extreme values of κ = +1 and κ = −1 indicate an asymmetrical peak with a heavy tail towards the right and left, respectively, while κ = 0 indicates a symmetric peak. In Fig. 6, the distributions of this value are visualized as data points and as violin plots: All calculated skews are presented in the Table S4 (ESI†).

For the hydrogen atoms in the UiO-66 without CO_2 adsorption, all shielding tensors exhibit heavy tails in the right direction (most signals have κ = 0.53 and three have κ = 1.0), as shown in Fig. 6(a) (right-end). A similar feature is observed when one CO_2 molecule is adsorbed at Site I or III. When one CO_2 molecule is adsorbed at Site II, however, several peaks exhibit smaller skew ($0 < \kappa < 0.5$). None of the proton peaks has negative skew. When fifteen CO_2 molecules are adsorbed, six new signals with skew near 0.1 appear, while the others mainly take on more intermediate values between the initial κ = 0.5 and κ = 1.0. These results suggest that CO_2 adsorption is difficult to detect *via* the skew of H signals, with the main effect of adsorption at Site II being the appearance of more symmetric peaks.

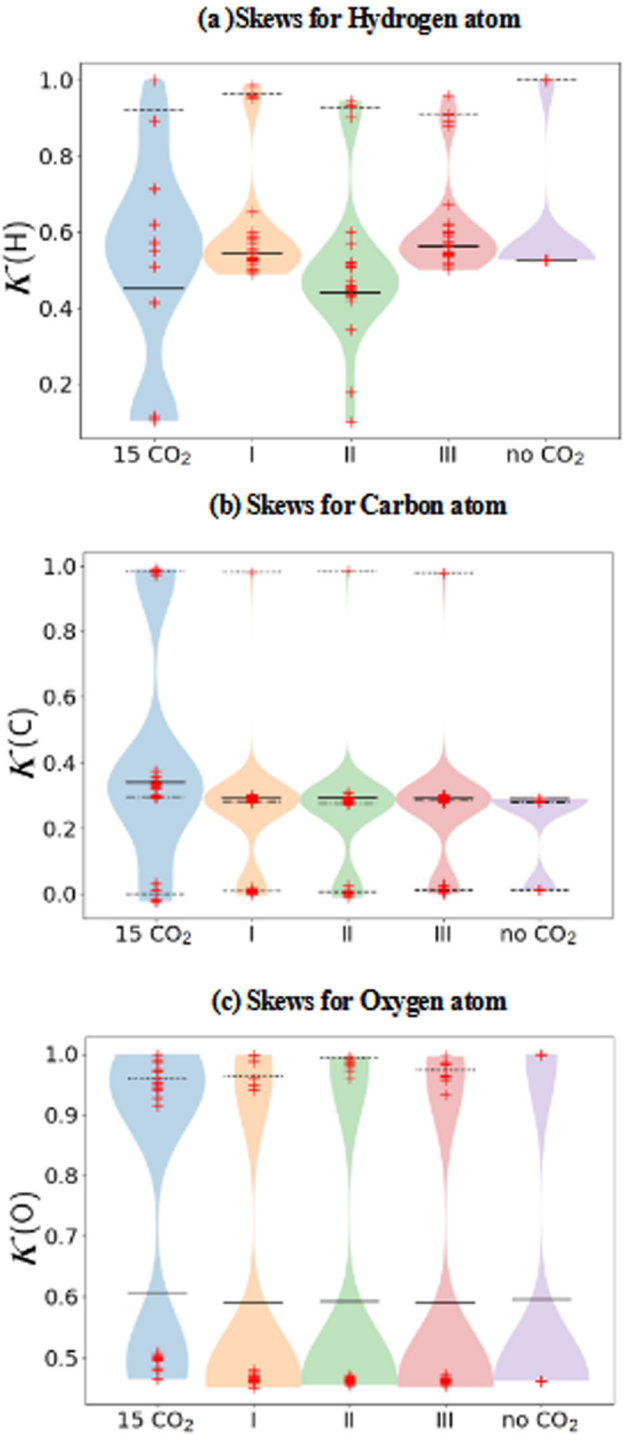

Fig. 6 The skew of hydrogen (left), carbon (middle), oxygen (right) atoms in CO_2 with UiO-66. The leftmost distribution is for UiO-66 with fifteen CO_2. The next three are for one CO_2 at Site I, II, and III, respectively. The rightmost distribution is for UiO-66 without CO_2. Data points are shown as crosses. The horizontal solid, dashed, dash-dotted, and dotted lines show mean values for different chemical groupings of the atoms.

The anisotropy of the carbon NMR shielding constants in UiO-66 without CO_2 exhibits a smaller skew ($0 < \kappa < 0.3$) than does the hydrogen shielding constant (Fig. 6(b); right-end). These values are consistent with the small skews of carbon NMR signals reported previously (Fig. 2a in ref. 67). When one CO_2 molecule is adsorbed at Site I, II, or III, its carbon NMR shielding constants show very large skew around $\kappa \approx +1$ (Fig. 6(b); middle results). This remains the same when fifteen CO_2 molecules are adsorbed (Fig. 6(b); left-end result). However, for the carbons in UiO-66, the skews are insensitive to adsorption of fifteen CO_2 molecules except for a moderate shift from 0.3 to around 0.35. On the other hand, the oxygen shielding constants of UiO-66 are concentrated at two positive skews $\kappa = 0.46$ and $\kappa = 1.0$ when no CO_2 is adsorbed (right-end of Fig. 6(c)). Adsorption of CO_2 perturbs these UiO-66 values and adds new signals with nearly maximal skew κ around 0.9. The resulting broadening of the skew distribution is clearly shown in the violin plot (Fig. 6(c); middles and left-end results).

In summary, the skews of carbon and oxygen NMR peaks change considerably upon the adsorption of fifteen CO_2 molecules, whereas the skews of hydrogen NMR peaks change moderately. NMR line shapes of carbon and oxygen atoms are useful for investigating CO_2 adsorption, although the carbon and oxygen NMR shielding constants are not very sensitive to CO_2 adsorption, as described above.

Conclusions

In this work, we investigated adsorption of carbon dioxide, acetone and methanol to UiO-66 using a CM/PM-combined method consisting of DFT calculation on infinite UiO-66 under periodic boundary condition and post-Hartree–Fock (SCS-MP2 and MP2.5) calculations on cluster models. The adsorption of fifteen to sixteen CO_2 molecules occurs at three sites. One molecule is adsorbed at each μ-OH group bridging three Zr atoms (Site I); in total, three or four CO_2 molecules are adsorbed at Site I, maybe depending on the pressure. Six CO_2 molecules are adsorbed around the pillar ligand, where each molecule is loosely surrounded by three terephthalate ligands (Site II). Further six molecules are adsorbed around the pillar ligand, where the gas molecule is surrounded well by three terephthalate ligands (Site III). Methanol and acetone are adsorbed at Sites I, II, and III in the similar manner to CO_2. The adsorption energy decreases in the order Site I > Site III > Site II for all three gas molecules. The strongest adsorption occurs at Site I. At this site, the protonic hydrogen atom of the μ-OH group bridging three Zr atoms interacts with the oxygen atom of gas molecule through a Brønsted-acid–Lewis-base interaction. This is the reason why the particularly large adsorption energy is obtained at Site I. At Site I, the binding energy decreases in the order acetone > methanol > CO_2 because the negative charge of the oxygen atom decreases in the order acetone > methanol ≫ CO_2. This Site I is effective for adsorption of gas molecule with negatively charged atom and/or Lewis base moiety. At Sites II and III, the adsorption occurs by weak interactions; the electrostatic interactions of the oxygen atom of the gas molecule with the hydrogen atoms of the C_6H_4 ring and carboxyl carbon atom and several dispersion interactions in the CO_2 adsorption, the CH–π interaction and electrostatic interaction between the methyl hydrogen atoms of the gas molecule and the oxygen atoms of the ligand in the acetone adsorption, and the OH–π interaction and the electrostatic interaction between the protonic hydrogen atom of the methanol OH group and the oxygen atoms of the carboxyl group of the ligand in the methanol adsorption.

The post-Hartree–Fock correction decreases the adsorption energy by 4% at Site I when the HO–Zr moiety is involved in the correction, 9% when the HO–Zr moiety is not involved in the correction, 29% at Site II, and 11% at Site III in the CO_2 adsorption case. The correction of BE at Site I is small because the Brønsted-acid–Lewis-base interaction including the electrostatic interaction between the negatively charged oxygen atom of CO_2 and the positively charged hydrogen atom of the μ-OH group largely contributes to the adsorption energy at Site I. It is likely that the larger post-Hartree–Fock correction at Site II is attributable to the CO_2 adsorption structure in which the CO_2 exists at a rather short distance from the C_6H_4 ring of the terephthalate ligand but the CO_2 π orbitals deviate from that of the C_6H_4 ring; because such a deviated position leads to smaller dispersion and π–π interactions, post-Hartree–Fock methods are needed for a correct evaluation of the binding energy.

Because CO_2 adsorption to MOFs is a promising technique for CO_2 capture from combustion gases, we focus on to what extent NMR measurements of hydrogen, carbon, and oxygen atoms provide meaningful information on CO_2 adsorption. The isotropic shielding constant of the hydrogen atom significantly differs among adsorptions of no CO_2, one CO_2 (at Site I, II, or III), and fifteen CO_2 molecules (Sites I to III). Although the isotropic carbon and oxygen NMR shielding constants do not change very much by CO_2 adsorption, their skews depend on CO_2 adsorption, indicating that the carbon and oxygen NMR measurements are also useful for investigating the CO_2 adsorption. These results strongly suggest that NMR spectroscopy is a promising experimental tool for investigating CO_2 adsorption to UiO-66.

Conflicts of interest

The authors declare no competing financial interest.

Acknowledgements

This work was supported by JST-CREST (JPMJCR20B6), JSPS Grant-in-aid for Scientific Research (JPJSBP1 20199902). We wish to thank Research Center for Computational Science in National Institutes of Natural Sciences (NINS), Okazaki, Japan for the use of Super Computers (Project: 22-IMS-C003), UNINETT Sigma2 – the National Infrastructure for High Performance Computing and Data Storage for providing computational

resources, and the Center of Excellence Hylleraas Center for Quantum Molecular Sciences (Grant No. 262695) in Norway.

References

1 J. H. Cavka, S. Jakobsen, U. Olsbye, N. Guillou, C. Lamberti, S. Bordiga and K. P. Lillerud, *J. Am. Chem. Soc.*, 2008, **130**, 13850–13851.

2 M. Kandiah, M. H. Nilsen, S. Usseglio, S. Jakobsen, U. Olsbye, M. Tilset, C. Larabi, E. A. Quadrelli, F. Bonino and K. P. Lillerud, *Chem. Mater.*, 2010, **22**, 6632–6640.

3 L. Valenzano, B. Civalleri, S. Chavan, S. Bordiga, M. H. Nilsen, S. Jakobsen, K. P. Lillerud and C. Lamberti, *Chem. Mater.*, 2011, **23**, 1700–1718.

4 M. Kandiah, S. Usseglio, S. Svelle, U. Olsbye, K. P. Lillerud and M. Tilset, *J. Mater. Chem.*, 2010, **20**, 9848–9851.

5 S. Yuan, J. Qin, C. Lollar and H. Zhou, *Chem. Rev.*, 2014, **114**, 10575–10612.

6 D. Zou and D. Liu, *Mater. Today Chem.*, 2019, **12**, 139–165.

7 N. Hanikel, M. S. Prévot and O. M. Yaghi, *Nat. Nanotechnol.*, 2020, **15**, 348–355.

8 M. Wu, Q. Zhang, Q. Zhang, H. Wang, F. Wang, J. Liu, L. Guo and K. Song, *Front. Chem.*, 2022, **10**, 842894.

9 J. Winarta, B. Shan, S. M. Mcintyre, L. Ye, C. Wang, J. Liu and B. Mu, *Cryst. Growth Des.*, 2019, **20**, 1347–1362.

10 M. Usman, A. Helal, M. M. Abdelnaby, A. M. Alloush, M. Zeama and Z. H. Yamani, *Chem. Rec.*, 2021, **21**, 1771–1791.

11 X. Feng, H. S. Jena, C. Krishnaraj, K. Leus, G. Wang, H. Chen, C. Jia and P. Van Der Voort, *ACS Appl. Mater. Interfaces*, 2021, **13**, 60715–60735.

12 F. Ahmadijokani, H. Molavi, M. Rezakazemi, S. Tajahmadi, A. Bahi, F. Ko, T. M. Aminabhavi, J.-R. Li and M. Arjmand, *Prog. Mater. Sci.*, 2022, **125**, 100904.

13 S. Kitagawa, R. Kitaura and S.-I. Noro, *Angew. Chem., Int. Ed.*, 2004, **43**, 2334–2375.

14 D. K. Wanigarathna, J. Gao and B. Liu, *Mater. Adv.*, 2020, **1**, 310–320.

15 T. Wang, E. Lin, Y.-L. Peng, Y. Chen, P. Cheng and Z. Zhang, *Coord. Chem. Rev.*, 2020, **423**, 213485.

16 J.-R. Li, R. J. Kuppler and H.-C. Zhou, *Chem. Soc. Rev.*, 2009, **38**, 1477–1504.

17 T. Pham, K. A. Forrest, D. M. Franz and B. Space, *CrystEngComm*, 2017, **19**, 4646–4665.

18 Z. Zhai, X. Zhang, X. Hao, B. Niu and C. Li, *Adv. Mater. Technol.*, 2021, **6**, 2100127.

19 H. R. Abid, H. Tian, H.-M. Ang, M. O. Tade, C. E. Buckley and S. Wang, *J. Chem. Eng.*, 2012, **187**, 415–420.

20 O. G. Nik, X. Y. Chen and S. Kaliaguine, *J. Membr. Sci.*, 2012, **413**, 48–61.

21 C. Chen, Y.-R. Lee and W.-S. Ahn, *J. Nanosci. Nanotechnol.*, 2016, **16**, 4291–4301.

22 J. Liu, P. K. Thallapally, B. P. McGrail, D. R. Brown and J. Liu, *Chem. Soc. Rev.*, 2012, **41**, 2308–2322.

23 S. Shalini, S. Nandi, A. Justin, R. Maity and R. Vaidhyanathan, *Chem. Commun.*, 2018, **54**, 13472–13490.

24 L. Li, H. S. Jung, J. W. Lee and Y. T. Kang, *Renewable Sustainable Energy Rev.*, 2022, **162**, 112441.

25 Y.-S. Bae and R. Q. Snurr, *Angew. Chem., Int. Ed.*, 2011, **50**, 11586–11596.

26 H. Li and M. R. Hill, *Acc. Chem. Res.*, 2017, **50**, 778–786.

27 H. Jasuja, J. Zang, D. S. Sholl and K. S. Walton, *J. Phys. Chem. C*, 2012, **116**, 23526–23532.

28 Q. Yang, S. Vaesen, F. Ragon, A. D. Wiersum, D. Wu, A. Lago, T. Devic, C. Martineau, F. Taulelle, P. L. Llewellyn, H. Jobic, C. Zhong, C. Serre, G. De Weireld and G. Maurin, *Angew. Chem., Int. Ed.*, 2013, **39**, 10316–10320.

29 M. Younas, M. Rezakazemi, M. Daud, M. B. Wazir, S. Ahmad, N. Ullah, Inamuddin and S. Ramakrishna, *Prog. Energy Combust.*, 2020, **80**, 100849.

30 H. Chevreau, W. Liang, G. J. Kearley, S. G. Duyker, D. M. D'Alessandro and V. K. Peterson, *J. Phys. Chem. C*, 2015, **119**, 6980–6987.

31 A. Nandy, A. C. Forse, V. J. Witherspoon and J. A. Reimer, *J. Phys. Chem. C*, 2018, **122**, 8295–8305.

32 Materials Studio, BIOVIA Inc., San Diego, California, USA, 2013.

33 A. K. Rappé, C. J. Casewit, K. Colwell, W. A. Goddard III and W. M. Skiff, *J. Am. Chem. Soc.*, 1992, **114**, 10024–10035.

34 A. K. Rappe and W. A. Goddard III, *J. Phys. Chem.*, 1991, **95**, 3358–3363.

35 Q. Yang, D. Liu, C. Zhong and J.-R. Li, *Chem. Rev.*, 2013, **113**, 8261–8323.

36 S. Zuluaga, P. Canepa, K. Tan, Y. J. Chabal and T. Thonhauser, *J. Condens. Matter Phys.*, 2014, **26**, 133002.

37 J. P. Perdew, K. Burke and M. Ernzerhof, *Phys. Rev. Lett.*, 1996, **77**, 3865.

38 S. Grimme, *J. Comput. Chem.*, 2004, **25**, 1463–1473.

39 S. Grimme, J. Antony, S. Ehrlich and H. Krieg, *J. Chem. Phys.*, 2010, **132**, 154104.

40 U. Ryde, R. A. Mata and S. Grimme, *Dalton Trans.*, 2011, **40**, 11176–11183.

41 P. E. Blöchl, *Phys. Rev. B: Condens. Matter Mater. Phys.*, 1994, **50**, 17953.

42 G. Kresse and D. Joubert, *Phys. Rev. B: Condens. Matter Mater. Phys.*, 1999, **59**, 1758.

43 G. Kresse and J. Furthmüller, *Comput. Mater. Sci.*, 1996, **6**, 15–50.

44 G. Kresse and J. Furthmüller, *Phys. Rev. B: Condens. Matter Mater. Phys.*, 1996, **54**, 11169.

45 K. Sillar and J. Sauer, *J. Am. Chem. Soc.*, 2012, **134**, 18354–18365.

46 A. Kundu, G. Piccini, K. Sillar and J. Sauer, *J. Am. Chem. Soc.*, 2016, **138**, 14047–14056.

47 J.-J. Zheng, S. Kusaka, R. Matsuda, S. Kitagawa and S. Sakaki, *J. Am. Chem. Soc.*, 2018, **140**, 13958–13969.

48 C. Gu, N. Hosono, J.-J. Zheng, Y. Sato, S. Kusaka, S. Sakaki and S. Kitagawa, *Science*, 2019, **363**, 387–391.

49 J.-J. Zheng and S. Sakaki, *J. Photochem. Photobiol., C*, 2022, **51**, 100482.

50 S. Dapprich, I. Komáromi, K. S. Byun, K. Morokuma and M. J. Frisch, *THEOCHEM*, 1999, **461**, 1–21.

51 L. W. Chung, W. Sameera, R. Ramozzi, A. J. Page, M. Hatanaka, G. P. Petrova, T. V. Harris, X. Li, Z. Ke, F. Liu, H.-B. Li, L. Ding and K. Morokuma, *Chem. Rev.*, 2015, **115**, 5678–5796.

52 S. Grimme, *J. Chem. Phys.*, 2003, **118**, 9095–9102.

53 S. Grimme, *J. Phys. Chem. A*, 2005, **109**, 3067–3077.

54 K. E. Riley, M. Pitonák, P. Jurecka and P. Hobza, *Chem. Rev.*, 2010, **110**, 5023–5063.

55 M. M. Deshmukh and S. Sakaki, *J. Comput. Chem.*, 2012, **33**, 617–628.

56 D. Andrae, U. Haeussermann, M. Dolg, H. Stoll and H. Preuss, *Theor. Chim. Acta*, 1990, **77**, 123–141.

57 S. F. Boys and F. Bernardi, *Mol. Phys.*, 1970, **19**, 553–566.

58 M. J. Frisch, G. W. Trucks, H. B. Schlegel, G. E. Scuseria, M. A. Robb, J. R. Cheeseman, G. Scalmani, V. Barone, G. A. Petersson, H. Nakatsuji, X. Li, M. Caricato, A. V. Marenich, J. Bloino, B. G. Janesko, R. Gomperts, B. Mennucci, H. P. Hratchian, J. V. Ortiz, A. F. Izmaylov, J. L. Sonnenberg, D. Williams-Young, F. Ding, F. Lipparini, F. Egidi, J. Goings, B. Peng, A. Petrone, T. Henderson, D. Ranasinghe, V. G. Zakrzewski, J. Gao, N. Rega, G. Zheng, W. Liang, M. Hada, M. Ehara, K. Toyota, R. Fukuda, J. Hasegawa, M. Ishida, T. Nakajima, Y. Honda, O. Kitao, H. Nakai, T. Vreven, K. Throssell, J. A. Montgomery, Jr., J. E. Peralta, F. Ogliaro, M. J. Bearpark, J. J. Heyd, E. N. Brothers, K. N. Kudin, V. N. Staroverov, T. A. Keith, R. Kobayashi, J. Normand, K. Raghavachari, A. P. Rendell, J. C. Burant, S. S. Iyengar, J. Tomasi, M. Cossi, J. M. Millam, M. Klene, C. Adamo, R. Cammi, J. W. Ochterski, R. L. Martin, K. Morokuma, O. Farkas, J. B. Foresman and D. J. Fox, *Gaussian 16 Revision A.03*, Gaussian Inc., Wallingford CT, 2016.

59 (a) These $BE^{PBE\text{-}D3:PBC}$ values were calculated as a difference between the $BE^{PBE\text{-}D3:PBC}$ values for the adsorption of sixteen CO_2 molecules and that for fifteen CO_2 molecules. These values are larger than the $BE^{PBE\text{-}D3:PBC}$ value for one CO_2 molecule, which is discussed below and shown in Table 1. It is likely that the larger $BE^{PBE\text{-}D3:PBC}$ values result from the CO_2–CO_2 van der Waals type attractive interactions. (b) The seventeenth CO_2 molecule is adsorbed at the new site. This site is distant from pillar ligand and the seventeenth CO_2 molecule is surrounded well by CO_2 molecules at site II. This new site is possible only here. It is likely suggested that seventeen CO_2 molecules are adsorbed but the adsorption of more than seventeen CO_2 molecules is difficult to occur.

60 The powder sample was used for neutron powder diffraction (NPD) measurements followed by Rietveld refinement. See ref. 30.

61 The gas adsorption at Site III occurs with the dispersion interactions described below; the π–π interaction contributes to the CO_2 adsorption and the OH-π interaction contributes to the methanol adsorption. Although the CH bonds of methyl groups of acetone are considerably distant from the C_6H_4 ring, it is likely that the CH–π interaction contributes to the acetone adsorption because the CH bonds of two methyl groups exist at a good position for the CH–π interaction with the C_6H_4 ring.

62 C. H. Lau, R. Babarao and M. R. Hill, *Chem. Commun.*, 2013, **49**, 3634–3636.

63 A. Policicchio, M. Florent, A. Celzard, V. Fierro, J. Jagiello and T. J. Bandosz, *Microporous Mesoporous Mater.*, 2020, **309**, 110571.

64 The experimental value was estimated to be about 26 kJ mol^{-1} from Fig. 4 of ref. 62 and 22 kJ mol^{-1} from Fig. 9 of ref. 63.

65 H. Wu, Y. S. Chua, V. Krungleviciute, M. Tyagi, P. Chen, T. Yildirim and W. Zhou, *J. Am. Chem. Soc.*, 2013, **135**, 10525–10532.

66 Y. Ma, W. Lu, X. Han, Y. Chen, I. da Silva, D. Lee, A. M. Sheveleva, Z. Wang, J. Li, W. Li, M. Fan, S. Xu, F. Tuna, E. J. L. McInnes, Y. Cheng, S. Ruić, P. Manuel, M. D. Frogley, A. J. Ramirez-Cuesta, M. Schröder and S. Yang, *J. Am. Chem. Soc.*, 2022, **144**, 8624–8632.

67 S. Devautour-Vinot, G. Maurin, C. Serre, P. Horcajada, D. Paula da Cunha, V. Guillerm, E. de Souza Costa, F. Taulelle and C. Martineau, *Chem. Mater.*, 2012, **24**, 2168–2177.

68 P. He, J. Xu, V. V. Terskikh, A. Sutrisno, H.-Y. Nie and Y. Huang, *J. Phys. Chem. C*, 2013, **117**, 16953–16960.

69 J. Mason, *Solid State Nucl. Magn. Reson.*, 1993, **2**, 285–288.